Electronic Supporting Information

In-situ coating amorphous boride on ternary pyrite-type boron sulfide for highly efficient oxygen evolution

Tingting Li, Tianyun Jing, Dewei Rao, Xiaotian Jia, Yunpeng Zuo*, Štěpán Kment, Radek Zbořil*

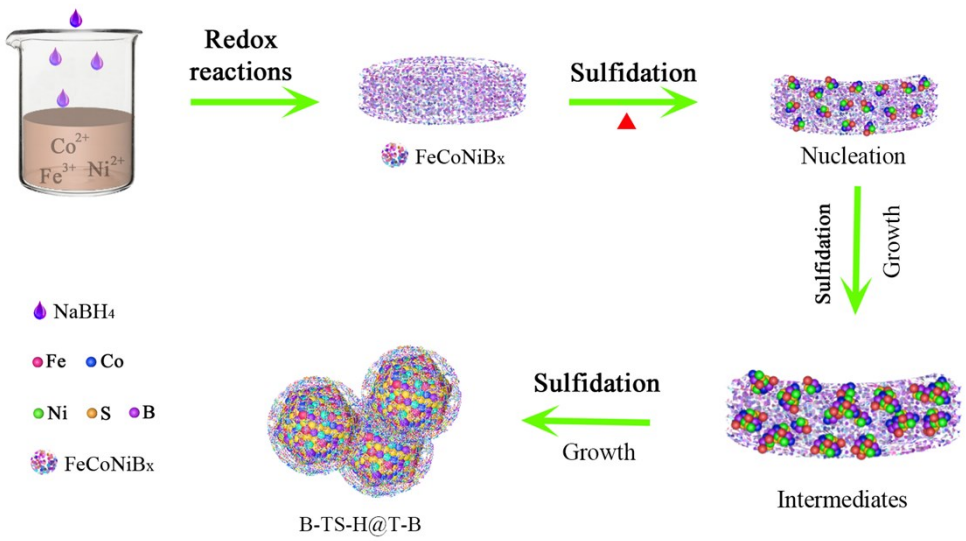

Scheme S1. Schematic illustration of the B-TS-H@T-B through two step, redox reaction and sulfidation. The red, blue, green, yellow and purple spheres represent Fe, Co, Ni, S and B atoms, respectively.

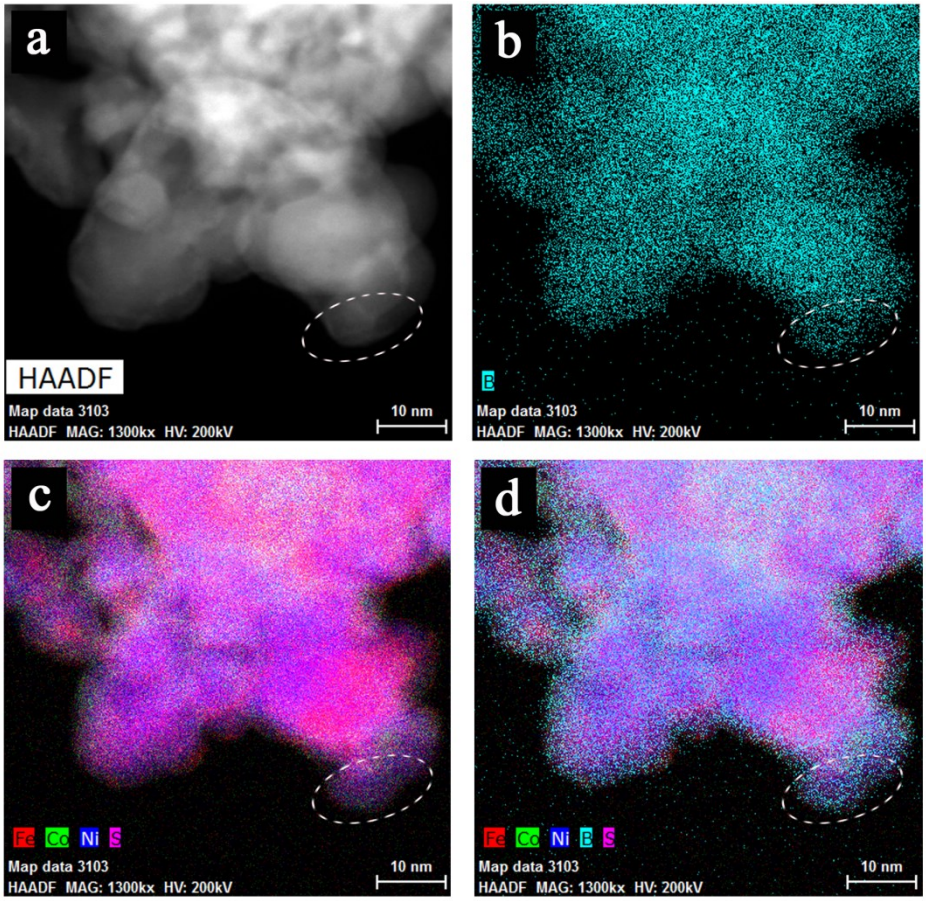

Figure S1. a) The HAADF-STEM and b,c,d) the corresponding TEM-EDX elemental mapping images of B-TS-H@T-B.

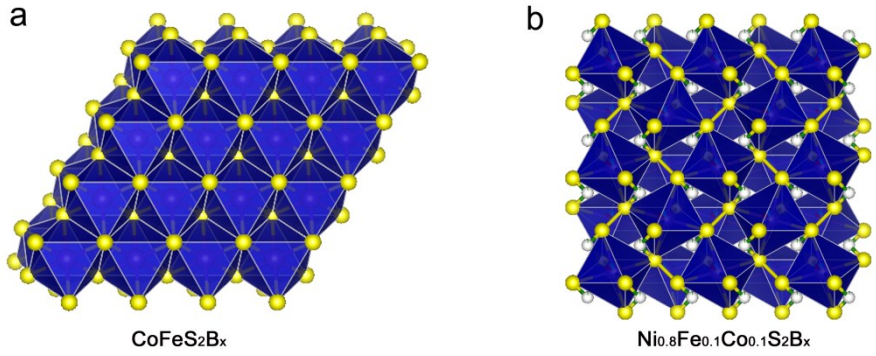

Figure S2. a,b) Polyhedral illustration structure of the $CoFeS_2B_x$ and $Ni_{0.8}Fe_{0.1}Co_{0.1}S_2B_x$.

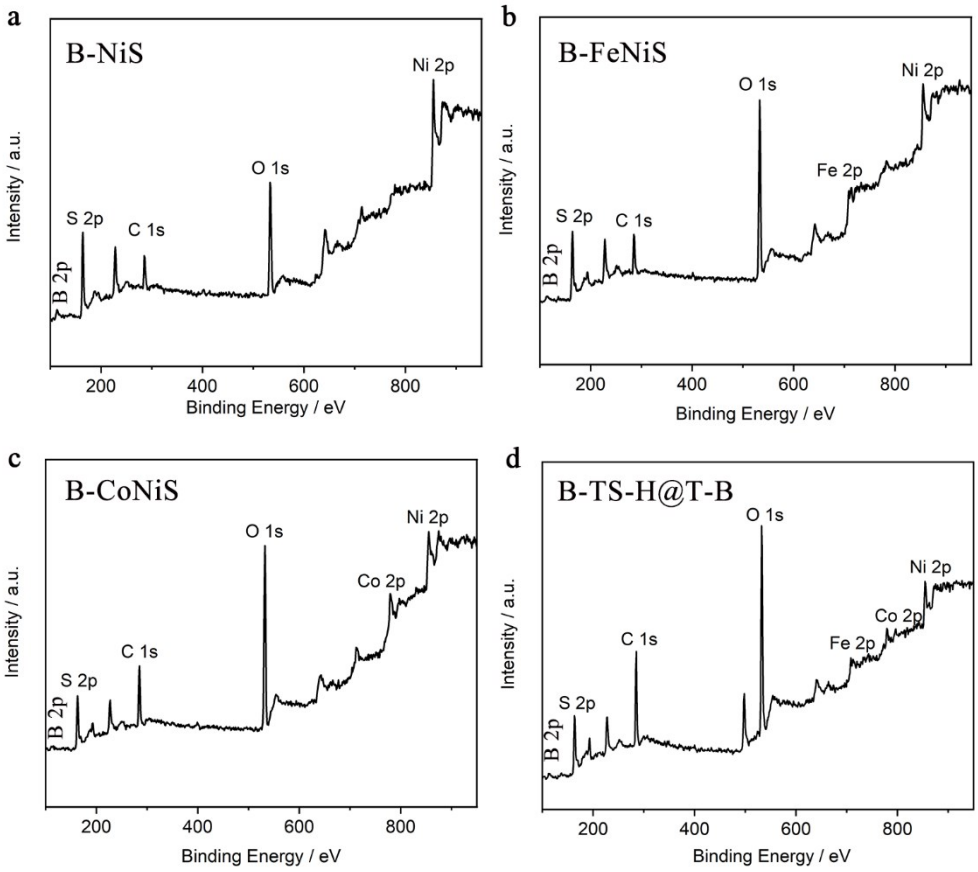

Figure S3. XPS spectra of (a) B-NiS, (b) B-FeNiS, (c) B-CoNiS, (d) B-TS-H@T-B.

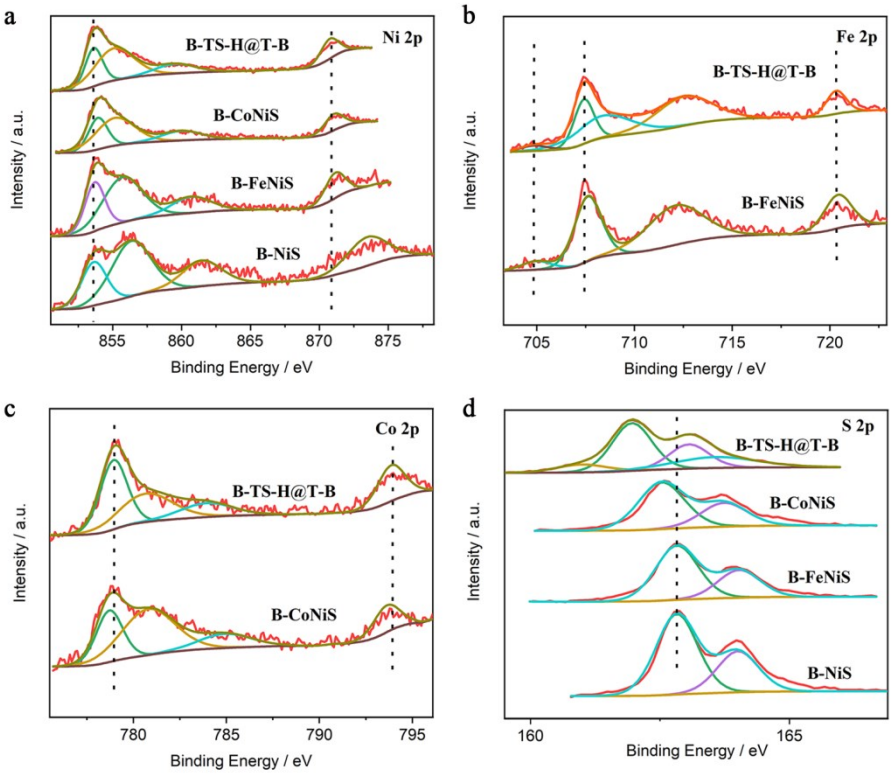

Figure S4. The high-resolution XPS of Ni 2p (a), Fe 2p (b), Co 2p (c) and S 2p (d).

The results in Figure S3 demonstrate the corresponding existence elements in B-NiS, B-CoNiS, B-FeNiS and B-TS-H@T-B, including B, Ni and S. The high-resolution Fe 2p, Co 2p, Ni 2p and S 2p XPS regions present in the Figure S4. For the Ni 2p XPS spectrum of B-TS-H@T-B, one pair of main peaks located at 853.78 and 870.88 eV are assigned to Ni^{2+} $2p_{3/2}$ and $2p_{1/2}$. It's obviously that the binding energy of Ni 2p gradually decreases as the increase of metal elements from B-NiS to B-TS-H@T-B, due to the emergence of multivalent metals. Additionally, the two peaks of Fe $2p_{3/2}$ and Fe $2p_{1/2}$ in B-FeNiS (707.48 eV, 720.48 eV) shift to 707.38 eV, 720.28 eV in B-TS-H@T-B (Figure S4b), which reveals the bond ability of the metals become weaken as the electron density of the metal site changed. The peaks shift in S 2p XPS section indicate the exposure of electron-deficient metal sites in B-TS-H@T-B.

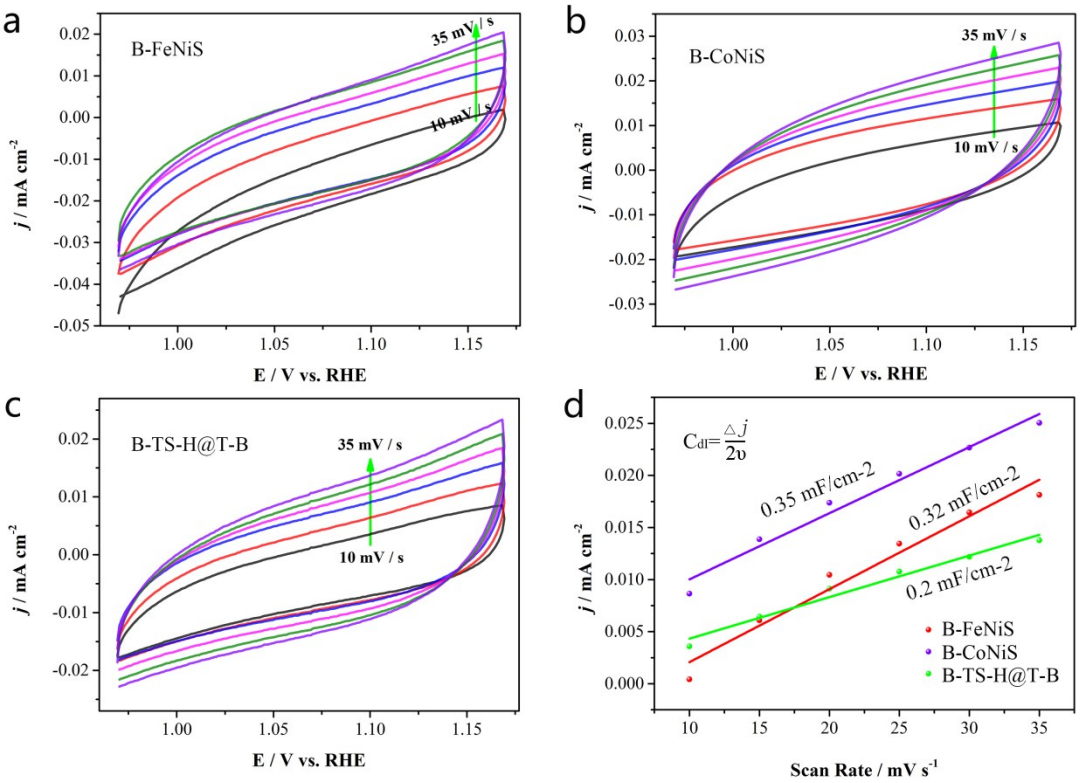

Figure S5. CVs under different scan rates of a) B-FeNiS, b) B-CoNiS, c) B-TS-H@T-B, and d) Scan rate dependent-current densities of the B-FeNiS, B-CoNiS, B-TS-H@T-B. υ is the scan rate.

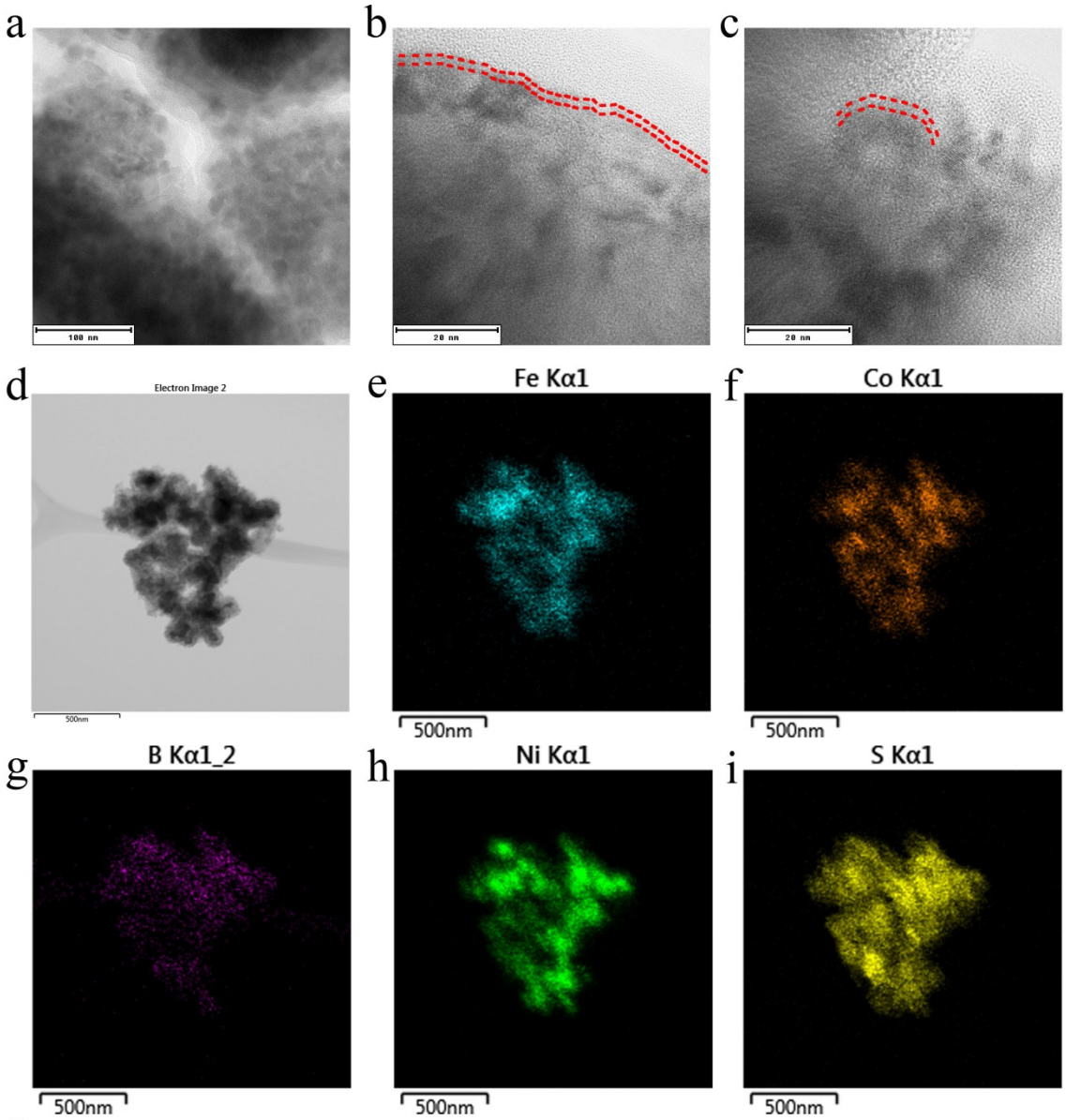

Figure S6. (a, b, c) Enlarged HRTEM images of the B-TS-H@T-B after OER test. (d-i) Typical HRTEM image of B-TS-H@T-B after stability test and the corresponding EDS mapping images Co, Ni, B, Fe and S.

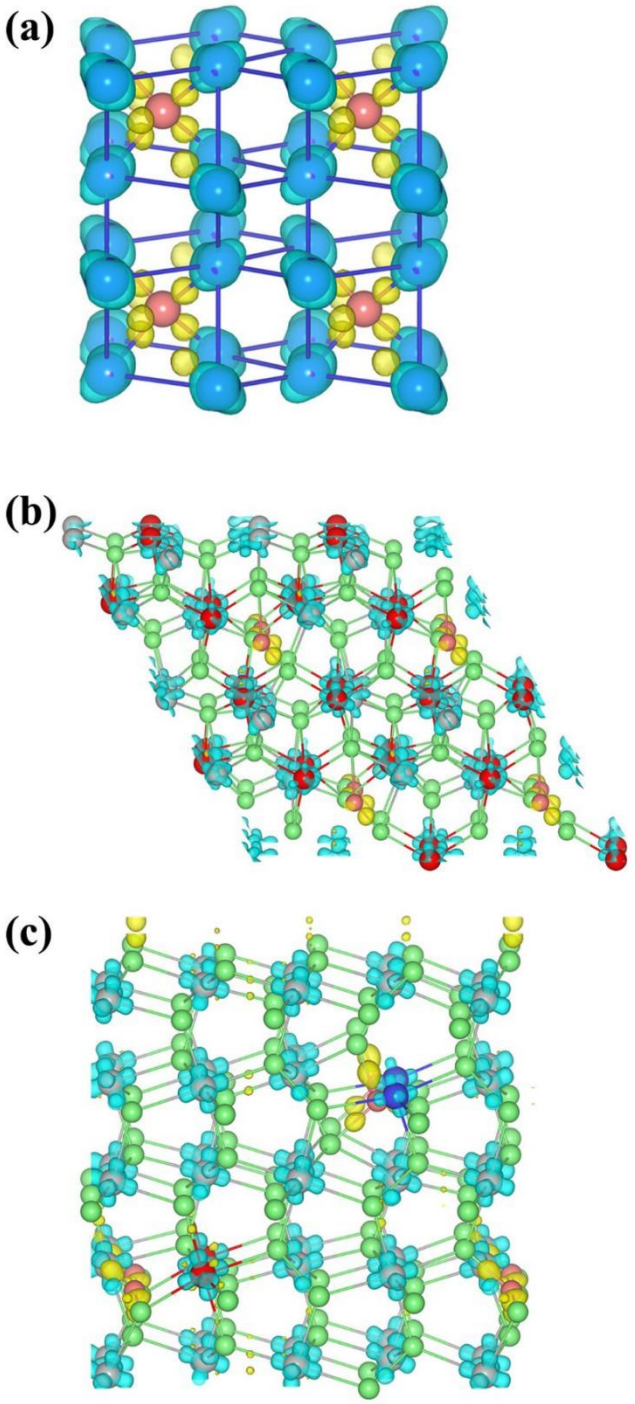

Figure S7. The deformantion charge density of B-doped samples. a) NiBx, b) $CoFeS_2B_x$, and c) $FeCoNiSB_x$. The Ni is blue ball, Fe is red ball, Co is gray ball, S is green ball and B is pink ball. The yellow areas represent the charge accumulation, and cavy areas represent the charge depletion.

Table S1. The comparison of the overpotentials at 10 mA cm^{-2} for OER of reported catalysts recently.

Catalysts	Overpotential (mV) at 10 mA cm^{-2}	References
B-TS-H@T-B	344.4 mV	Our work
RhO_2	~385 mV	1
IrO_2	~320 mV	2
S, N-CNTs/CoS_2@Co	340 mV	3
Co_9S_8@MoS_2	342 mV	4
Co_9S_8@MoS_2/CNFs	430 mV	5
Co-P films	345 mV	6
CoNC/CNF	430 mV	7
CoNC@MoS_2 /CNFs	350 mV	7
CoS-$Co(OH)_2$@aMoS_{2+x}/ ni foam	380 mV	8
NiCoS/$Ti_3C_2T_x$	356 mV	9
Al_2Pt	450 mV (0.1 M $HClO_4$)	10
Co_8Ag oxide	370 mV	11

Table S2. The comparison of the overpotentials at 100 mA cm^{-2} for OER of reported catalysts recently.

Catalysts	Overpotential (mV) at 100 mA cm^{-2}	References
B-TS-H@T-B	419.4 mV	Our work
RhO_2	over 470 mV	1
IrO_2	over 570 mV	3
NCoM-SS-Ar	over 490 mV	12
Co_9S_8/Ni	~440 mV	13
S, N-CNTs/CoS_2@Co	~520 mV	3
c-Ti-Fe-S boxes	over 450 mV	14
c-Ti-Fe-S cubes	over 470 mV	14
Zn-Co-S NN/CFP	over 420 mV	15
Zn-Co-S NP/CFP	~470 mV	15
Zn-Co-S NS/CFP	over 490 mV	15
H-Fe-CoMoS	~350 mV	16
SNCF-NR	over 420 mV	17
CoP/rGO-400	~510 mV	18

References

1 Y. Liu, X. Xie, G. Zhu, Y. Mao, Y. Yu, S. Ju, X. Shen, H. Pang, *J. Mater. Chem. A* 2019, **7**, 15851.

2 Y. Liu, S. Yin, P. K. Shen, *ACS Appl. Mater. Interfaces* 2018, **10**, 23131.

3 J.-Y. Wang, T. Ouyang, N. Li, T. Ma, Z.-Q. Liu, *Sci. Bull.* 2018, **63**, 1130.

4 J. Bai, T. Meng, D. Guo, S. Wang, B. Mao, M. Cao, *ACS Appl. Mater. Interfaces* 2018, **10**, 1678.

5 H. Zhu, J. Zhang, R. Yanzhang, M. Du, Q. Wang, G. Gao, J. Wu, G. Wu, M. Zhang, B. Liu, J. Yao, X. Zhang, *Adv. Mater.* 2015, **27**, 4752.

6 N. Jiang, B. You, M. Sheng, Y. Sun, *Angew. Chem. Int. Ed.* 2015, **54**, 6251.

7 D. Ji, S. Peng, L. Fan, L. Li, X. Qin, S. Ramakrishna, *J. Mater. Chem. A* 2017, **5**, 23898.

8 T. Yoon, K. S. Kim, *Adv. Funct. Mater.* 2016, **26**, 7386.

9 H. Zou, B. He, P. Kuang, J. Yu, K. Fan, *ACS Appl. Mater. Interfaces* 2018, **10**, 22311.

10 I. Antonyshyn, A. M. Barrios Jimenez, O. Sichevych, U. Burkhardt, I. Veremchuk, M. Schmidt, A. Ormeci, I. Spanos, A. Tarasov, D. Teschner, G. Algara-Siller, R. Schlogl, Y. Grin, *Angew. Chem. Int. Ed.* 2020, **59**, 16770.

11 M. Yu, G. H. Moon, R. G. Castillo, S. DeBeer, C. Weidenthaler, H. Tuysuz, *Angew. Chem. Int. Ed.* 2020, **59**, 16544.

12 R. Gond, D. K. Singh, M. Eswaramoorthy, P. Barpanda, *Angew. Chem. Int. Ed.* 2019, **58**, 8330.

13 J. Li, W. Xu, J. Luo, D. Zhou, D. Zhang, L. Wei, P. Xu, D. Yuan, *Nanomicro Lett* 2018, **10**, 6.

14 J. Nai, Y. Lu, X.-Y. Yu, *J. Mater. Chem. A* 2018, **6**, 21891.

15 X. Wu, X. Han, X. Ma, W. Zhang, Y. Deng, C. Zhong, W. Hu, *ACS Appl. Mater. Interfaces* 2017, **9**, 12574.

16 Y. Guo, X. Zhou, J. Tang, S. Tanaka, Y. V. Kaneti, J. Na, B. Jiang, Y. Yamauchi, Y. Bando, Y. Sugahara, *Nano Energy* 2020, **75**, 104913.

17 Y. Zhu, W. Zhou, Y. Zhong, Y. Bu, X. Chen, Q. Zhong, M. Liu, Z. Shao, *Adv. Energy Mater.* 2017, **7**, 1602122.

18 L. Jiao, Y. X. Zhou, H. L. Jiang, *Chem. Sci.* 2016, **7**, 1690.